

# Evaluation of cloud properties in the NOAA/NCEP global forecast system using multiple satellite products

Hyelim Yoo · Zhanqing Li

Received: 15 July 2011 / Accepted: 19 June 2012  
© Springer-Verlag 2012

**Abstract** Knowledge of cloud properties and their vertical structure is important for meteorological studies due to their impact on both the Earth's radiation budget and adiabatic heating within the atmosphere. The objective of this study is to evaluate bulk cloud properties and vertical distribution simulated by the US National Oceanic and Atmospheric Administration National Centers for Environmental Prediction Global Forecast System (GFS) using three global satellite products. Cloud variables evaluated include the occurrence and fraction of clouds in up to three layers, cloud optical depth, liquid water path, and ice water path. Cloud vertical structure data are retrieved from both active (Cloud-Sat/CALIPSO) and passive sensors and are subsequently compared with GFS model results. In general, the GFS model captures the spatial patterns of hydrometeors reasonably well and follows the general features seen in satellite measurements, but large discrepancies exist in low-level cloud properties. More boundary layer clouds over the interior continents were generated by the GFS model whereas satellite retrievals showed more low-level clouds over oceans. Although the frequencies of global multi-layer clouds from observations

are similar to those from the model, latitudinal variations show discrepancies in terms of structure and pattern. The modeled cloud optical depth over storm track region and subtropical region is less than that from the passive sensor and is overestimated for deep convective clouds. The distributions of ice water path (IWP) agree better with satellite observations than do liquid water path (LWP) distributions. Discrepancies in LWP/IWP distributions between observations and the model are attributed to differences in cloud water mixing ratio and mean relative humidity fields, which are major control variables determining the formation of clouds.

**Keywords** Cloud fraction · NCEP global forecast system · Liquid water path · Ice water path · Cloud optical depth

## 1 Introduction

Clouds have been recognized as a major source of uncertainties in predicting global weather and estimating cloud feedbacks in the climate system (Stephens 2005). Weare et al. (1996) compared 24 model simulations of cloud amounts against the International Satellite Cloud Climatology Project (ISCCP) data. They found that global means of modeled high cloud amounts are about two to five times greater than those from satellite retrievals, whereas low-level cloud amounts were underestimated drastically. Zhang et al. (2005) compared the fraction of total, low-, mid- and high clouds from 10 general circulation models (GCMs) and 2 satellite products (ISCCP and the Clouds and Earth's Radiant Energy System (CERES)). While the total cloud amounts agree well, large discrepancies exist in cloud vertical structure among the models, and between satellite products.

Differentiating clouds in different layers is a challenging task for both satellite remote sensing and model simulation.

---

This paper is a contribution to the Topical Collection on Climate Forecast System Version 2 (CFSv2). CFSv2 is a coupled global climate model and was implemented by National Centers for Environmental Prediction (NCEP) in seasonal forecasting operations in March 2011. This Topical Collection is coordinated by Jin Huang, Arun Kumar, Jim Kinter and Annarita Mariotti.

---

H. Yoo · Z. Li  
Department of Atmospheric and Oceanic Science,  
University of Maryland, College Park, MD 20740, USA

Z. Li (✉)  
State Key Laboratory of Earth Surface Processes and Resource  
Ecology, GCESS, Beijing Normal University,  
Beijing 100875, China  
e-mail: zli@atmos.umd.edu

By virtue of their global coverage and long records, satellite data from passive sensors have been employed to detect global clouds, such as data from the Advanced Very High Resolution Radiometer (AVHRR) (Baum et al. 1995; Ou et al. 1996) and the Moderate Resolution Imaging Spectroradiometer (MODIS) (Baum and Spinhirne 2000). Taking advantage of MODIS channels, Chang and Li (2005a) proposed an algorithm that can identify single and cirrus-over-water dual-layer clouds. Applying their algorithm to global MODIS data, they obtained global multi-layer cloud distributions (Chang and Li 2005b). Thanks to the addition of a second layer of low clouds, their estimate of total low clouds over the globe is larger than all previous estimates based on passive sensors, but matches closely with space-borne lidar-based retrievals (see below).

Active remote sensing provides a better alternative to examine cloud vertical structure and their optical properties, as demonstrated by the CloudSat and the Cloud-Aerosol Lidar and Infrared Pathfinder Satellite Observations (CALIPSO) satellites which are a part of the A-Train satellite constellation. The 94-GHz radar onboard the CloudSat can penetrate through most cloud layers (Stephens et al. 2002). From CloudSat and CALIPSO, Mace et al. (2009) obtained the first global view of multi-layer clouds from active sensors. By simulating space-borne CloudSat radar signals, Bodas-Salcedo et al. (2008) evaluated clouds simulated by the UK Meteorological Office's global forecasting model.

There are two approaches evaluating model's performance with satellite observations: comparisons of cloud parameters between model simulations and satellite retrievals, and comparisons of radiances in satellite channels as observed by the satellite sensors and computed from model simulations. They have their strengths and weaknesses. The simulator approach circumvents the difficulties and uncertainties associated with retrievals of cloud parameters, but it suffers from some limitations as well. The same set of radiances may originate from different states of atmosphere and cloud, thus it is hard to pinpoint uniquely the exact sources of errors. The ISCCP simulator has been used to evaluate the performances of GCMs in simulating clouds (Zhang et al. 2005). The ISCCP simulator was validated against ground-based measurements (Mace et al. 2006). The MODIS simulator has a different treatment for partial cloudy pixels which affect the distributions of cloud and cloud optical depth (Pincus et al. 2012), apart from highly different channels.

Using datasets capable of detecting multi-layer clouds and their optical properties, we can evaluate cloud properties forecasted by the National Centers for Environmental Prediction (NCEP) Global Forecast System (GFS) model. Currently, many GCMs and weather forecasting models do not simulate cloud vertical structure very well on a global

scale (Bodas-Salcedo et al. 2008). The general spatial patterns of clouds are well-produced but the magnitudes and locations tend to differ more from observations.

In this paper, we examine the status of the 2007 version of the GFS model in generating clouds so that the representation of cloud processes might be objectively improved. Furthermore, the comparisons provide a general guidance for improving the capabilities of the GFS model in producing clouds by revealing model deficiencies in terms of both model output (clouds) and input (temperature, humidity, etc.). This paper is focused on the comparison of clouds from the GFS model and multiple satellite observations, while a separated paper includes investigation for the causes of the discrepancies.

Section 2 describes the various datasets used in this study and the methodology. The geographical distributions of different cloud parameters, analysis of the results, and comparisons of model output with several satellite retrievals are presented in Sect. 3. A summary is given in Sect. 4.

## 2 Data and methodology

### 2.1 Satellite retrievals

Data collected from the MODIS onboard the Terra (overpass time, 10:30 local time) satellite platform is used to extract cloud properties. The instrument has 36 onboard calibrated channels/bands (0.415–14.24  $\mu\text{m}$ ) (Barnes et al. 1998). Two sets of MODIS-based cloud products are employed here: the official operational product generated by the National Aeronautics and Space Administration (NASA) which is based on the algorithm developed originally by Platnick et al. (2003) with some subsequent revisions and a newly generated research product based upon the algorithm of Chang and Li (2005a). The two products are hereafter referred to as *MODIS-EOS* and *MODIS-CL*, respectively. Both datasets cover the period of January and July 2007. MODIS provides daily data covering the globe, data used in this study are for every day of a particular month.

The MODIS Level 2 cloud product, MOD06 (version Collection 5.1), used here includes the following variables at two spatial resolutions (1 km and 5 km): cloud-top pressure, cloud-top temperature, cloud phase, effective particle radius, and cloud optical depth (COD). Among these variables, effective particle radius and COD are derived at a 1-km resolution and averaged over  $1^\circ \times 1^\circ$  latitude-longitude grid boxes; monthly means are calculated for each grid box. All cloud variables based on satellite retrievals, except for COD, are classified as high, middle, or low according to cloud-top pressure. A mid-level cloud is identified when the cloud-top pressure falls between 350

and 642 mb which is the criterion used in identifying such clouds in the GFS model. For each cloud category, cloud fraction is calculated as the number of cloudy pixels in a grid box divided by the total number of pixels in that grid box. Like most passive cloud retrieval algorithms, the MODIS algorithm was based on the assumption of single-layer clouds in the retrieval of cloud properties. As such, the retrieved cloud top represents the top of the highest cloud regardless of the presence of any lower cloud layers.

The algorithm of Chang and Li (2005a) (hereafter the C–L algorithm) alleviates the problem because it can detect and retrieve cloud parameters for single-layer clouds and for thin-over-thick dual-layer clouds. Due to the frequent occurrence of such overlapped clouds, the C–L algorithm generates substantially more low clouds than the MODIS algorithm. The total amount of low clouds over oceans and over land retrieved from the C–L algorithm (MODIS product) is 34 % (22 %) and 28 % (16 %), respectively (Chang and Li 2005b). In addition to detecting more low clouds, the COD of the topmost layer and lower cloud in multi-layer clouds are differentiated using the C–L algorithm.

The CloudSat and CALIPSO satellites were launched in April 2006, carrying a 94-GHz cloud profiling radar (CPR) (Im et al. 2006) and a two-wavelength polarization sensitive lidar (Winker et al. 2007). These sensors are members of the A-Train afternoon constellation (Stephens et al. 2002), flying in a tight orbital formation so that all instruments probe the atmosphere within a few seconds of each other, rendering synergistic, simultaneous and independent information pertaining to cloud vertical structure. The lidar is capable of resolving very thin cirrus layers below 15 km to thicker cirrus clouds between 12 and 13 km while the radar is able to detect lower, more optically opaque cirrus clouds and can penetrate through much of deep convective clouds. Merged lidar-radar data offers the best compromise between the strengths and weaknesses of the two instrument retrieval methods (Mace et al. 2009). This combined dataset is called CloudSat–CALIPSO merged data (hereafter referred to as C–C satellites) which provides more detailed and more reliable cloud vertical structure information. This study uses the Level 2B Geoprof-lidar product (CloudSat CPR + CALIPSO Lidar Cloud mask) and the Level 2B TAU product for every day in January and July 2007. Up to a maximum of five different cloud layers can be output from C–C satellites and each layer has its individual cloud-top altitude and cloud-base altitude.

While the two active sensors provide the most direct and accurate measurement of cloud vertical structure, their horizontal coverage is much smaller than the wide swath ( $\sim 2,700$  km) of the MODIS imaging sensor which provides nearly global wall-to-wall coverage, except for data gaps at low latitudes. Both CloudSat and CALIPSO view the Earth in the nadir direction with footprints of 1.4 km and 1.1 km,

respectively. It is therefore necessary to use products from both passive and active sensors to complement each other's weaknesses/strengths. Because of the low spatial sampling rate, monthly mean values were computed for  $3^\circ \times 6^\circ$  lat/longitude grids for mapping in order to reduce the number of empty grids, as done in other studies using the product (Sassen and Wang 2008; Mace et al. 2009).

## 2.2 The GFS model

The GFS is a global weather prediction model run by the National Oceanic and Atmospheric Administration (NOAA). The GFS model has 64 vertical sigma-pressure hybrid layers and a T382 (equivalent to a nearly 35 km) horizontal resolution. GFS model grid 003 data are used in this study with a  $1^\circ \times 1^\circ$  latitude-longitude resolution. Output fields for a 1 day forecast generated at 3-h intervals (i.e., at 03, 06, 09, 12, 15, 18, 21, 24Z), starting from the control time of 00Z, are used. In other words, the forecasting data used here are from 00Z to 24Z for each day. Cloud properties output in each grid box are used for comparison with satellite retrievals over the domain covering  $60^\circ\text{S}–60^\circ\text{N}$  during January and July 2007. At high latitudes, the presence of bright snow and/or ice-covered surfaces leads to low accuracy in retrievals from passive sensors (Li and Leighton 1991), so data from those regions are not considered in this study. The GFS model fields were interpolated to satellite overpass times in order to match satellite retrievals. GFS model outputs include cloud cover, cloud-top pressure and height, and cloud-base pressure and height at high, middle and low levels of the atmosphere. High, middle, and low categories are defined with respect to cloud layer top pressure: less than 350 mb, between 350 mb and 642 mb, and greater than 642 mb, respectively.

### 2.2.1 GFS cloud fraction

The cloud fraction in a given grid box of the GFS model is computed using the parameterization scheme of Xu and Randall (1996):

$$C = \max \left[ R^{0.25} \left( 1 - \exp \left\{ \frac{2000 \times (q_c - q_{c\min})}{\min[\max\{[(1 - R) \times q^*]^{0.25}, 0.0001\}, 1.0]} \right\} \right), 0.0 \right], \quad (1)$$

where  $R$  is the relative humidity,  $q^*$  is the saturation specific humidity,  $q_c$  is the cloud water mixing ratio, and  $q_{c\min}$  is a minimum threshold value of  $q_c$ . Depending on the ambient temperature, the saturation specific humidity is calculated with respect to liquid or ice phase. Clouds in the GFS model are assumed to be maximum-randomly overlapped (<http://www.emc.ncep.noaa.gov/officenotes>).

### 2.2.2 GFS cloud optical depth (COD), effective radius (Re), liquid and ice water path (LWP and IWP)

The GFS model posts parameters for 21 vertically different layers. From the surface (1,000 mb) to the 900 mb level, the vertical resolution is 25 mb; less than 900 mb, there are 16 levels at a 50 mb resolution. Cloud phase is determined by the mean temperature ( $T_c$ ) of a cloud layer which is defined as the average of temperatures at the top and bottom of a cloud layer. If  $T_c$  is less than 258.16 K, the cloud layer is an ice cloud; otherwise, it is a water cloud.

Two methods have been used to parameterize cloud properties in the GFS model. The first method makes use of a diagnostic cloud scheme, in which cloud properties are determined based on model-predicted temperature, pressure, and boundary layer circulation from Harshvardhan et al. (1989). The diagnostic scheme is now replaced with a prognostic scheme that uses cloud water condensate information instead (<http://www.nws.noaa.gov/om/tpb/484.htm>).

For water clouds, a fixed value of 10  $\mu\text{m}$  for  $R_e$  is assumed over oceans and  $R_e$  values over land depend on temperature. Over land,  $R_e$  is defined as:

$$R_{ew} = -0.25 \times T_c + 73.29. \quad (2)$$

Its value ranges from 5  $\mu\text{m}$  to a maximum of 8.7  $\mu\text{m}$  for  $T_c$  of 258.16 K, below which cloud is treated as an ice cloud.

LWP is calculated using the following equation:

$$\text{LWP} = q \times \rho \times \Delta z, \quad (3)$$

where  $q$  is the cloud water mixing ratio in units of kg/kg,  $\rho$  is the density in  $\text{kg}/\text{m}^3$  (assumed to be constant), and  $\Delta z$  is the geopotential height thickness in units of m.

LWP and  $R_e$  information is used to calculate total column COD in the GFS model (Chou et al. 1998):

$$\tau_w = \text{LWP}(a_1 + (a_2/R_{ew})), \quad (4)$$

where LWP is given in units of  $\text{g}/\text{m}^2$ , and the coefficients  $a_1$  and  $a_2$  are given in Chou et al. (1998).

For ice clouds,  $R_e$  is calculated as empirical functions of ice water concentration and environmental temperature (Heymsfield and McFarquhar 1996):

$$\begin{aligned} R_{ei} &= (1250/9.917) \text{IWC}^{0.109} (T_c < 223.16 \text{ K}), \\ R_{ei} &= (1250/9.337) \text{IWC}^{0.080} (223.16 \text{ K} < T_c < 233.16 \text{ K}), \\ R_{ei} &= (1250/9.208) \text{IWC}^{0.055} (233.16 \text{ K} < T_c < 243.16 \text{ K}), \\ R_{ei} &= (1250/9.387) \text{IWC}^{0.031} (243.16 \text{ K} < T_c < 258.16 \text{ K}), \end{aligned} \quad (5)$$

where ice water concentration (IWC) is calculated as:

$$\text{IWC} = 1.371 \times 10^{(-14.0+0.04962 \times T_c)}. \quad (6)$$

IWP calculations are made in a similar manner. The COD for an ice cloud,  $\tau_i$ , is computed as:

$$\tau_i = \text{IWP}(a_3 + (a_4/R_{ei})), \quad (7)$$

where IWP is given in units of  $\text{g}/\text{m}^2$ , and the coefficients  $a_3$  and  $a_4$  are given in the GFS documentation. A total column COD in a particular grid box is obtained by summing water and ice CODs.

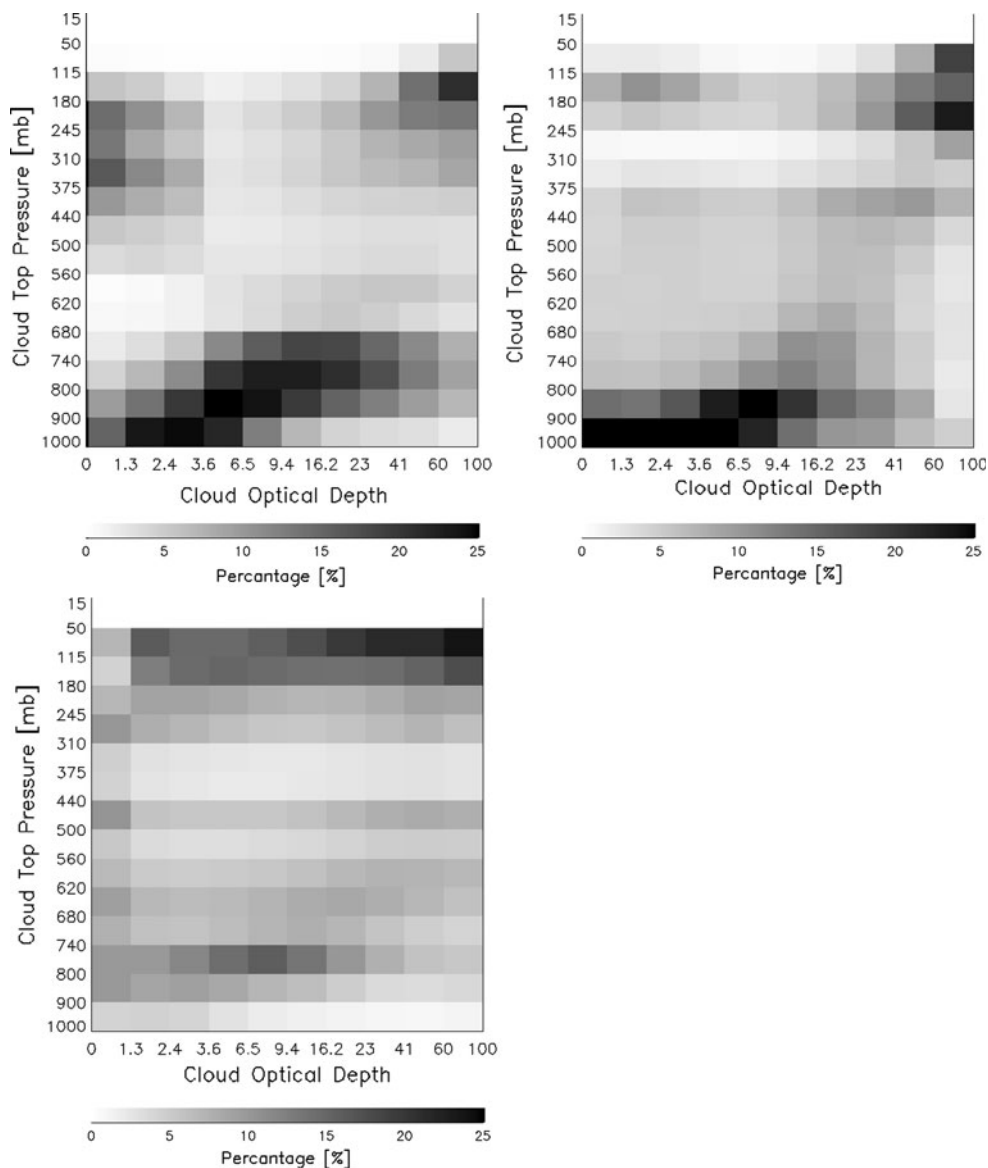
## 3 Results

### 3.1 Comparison of the two MODIS cloud products

Figure 1 shows comparisons of the joint histograms of cloud-top pressure and COD from MODIS-EOS, MODIS-CL, and the GFS model. In terms of the dominant modes at which clouds occur most frequently with particular ranges of cloud-top pressure and optical depth, three dataset exhibit rather distinct differences. The GFS results show one outstanding mode: deep convective clouds at high levels and a weak mode of low clouds. The MODIS-EOS shows a distinct bimodal distribution: deep thick clouds and low thin clouds. The MODIS-CL results reveal frequent occurrences of three dominant cloud types: optically thin cirrus clouds at high altitudes, optically thicker boundary layer clouds at lower levels, and deep convective clouds. In terms of cloud-top pressure alone, the two MODIS cloud products are similar in that both have two modes: high and low with rather low probability of clouds with tops in mid-layer around 500 mb. The MODIS-CL retrievals have more optically thin high clouds and less optically thick high clouds relative to the MODIS-EOS algorithm (see Fig. 1) because the former can differentiate overlapped thin cirrus over thick water clouds (Chang and Li 2005a, b). However, the total amount of high clouds (in terms of cloud-top pressure) in the MODIS-CL retrievals is the same as that retrieved from the MODIS-EOS algorithm (Chang and Li 2005b). The presence of overlapped cirrus over low clouds is the major cause for the differences which is further rooted to the assumption of single-layer cloud in the MODIS-EOS retrievals, leading to the general underestimation of low cloud amounts. In other words, many low clouds are missed because they are beneath the upper cirrus clouds that were not separated from single-layer clouds. Cirrus-over-water dual-layer clouds are identified as deep convective clouds for most cases based on passive sensors. Mistreatment of such overlapped clouds can lead to significant errors in estimating heating rates and longwave radiation because deep convective clouds and overlapped clouds have different effects on longwave radiation.

Due to the identification of both single and dual-layer clouds through exploitation of more MODIS channels, the C-L algorithm can identify such overlapped clouds except for those with uppermost cloud layers that are too thick

**Fig. 1** Joint histograms of cloud top pressure and cloud optical depth derived from near-global retrievals by applying the C–L algorithm (*top left panel*), the MODIS-EOS algorithm (*top right panel*), and the GFS model (*bottom left panel*) in July 2007



(CODs greater than 4.0). It is worth noting that the overall cloud-layer statistics of the MODIS-CL agree very well with those from a previous study using space-borne lidar measurements from the Geoscience Laser Altimeter System (GLAS) (Wylie et al. 2007). Coincidentally, the frequency of multi-layer clouds from both instruments is 27 % (see Table 1). In this sense, the capability in detecting multi-layer clouds by the C–L algorithm with passive MODIS data is similar to that of the laser-based active approach. Both can detect dual-layer clouds if the top clouds are optically thin, beyond which neither can penetrate.

### 3.2 Multi-layer cloud occurrence frequencies

Clouds in different vertical layers dictate the adiabatic heating rates and radiation balance of the atmospheric

column. Mistreatment of multi-layer clouds as single-layer cloud can lead to substantial errors in cloud amounts in different model layers, which could feedback to erroneous dynamics. Table 2 summarizes the global frequencies of occurrence of single-layer and multi-layer clouds from C–C satellites, MODIS-CL, and GFS model results. The frequency of single-layer, dual-layer, and multi-layer (three or more layers) clouds from C–C satellites in January (July) is 67.50 % (67.89 %), 26.58 % (25.98 %), and 5.92 % (6.13 %), respectively. The frequency of single-layer and dual-layer clouds from the MODIS-CL for the 2 months is 84.41 % (82.86 %) and 15.59 % (17.14 %), respectively. Frequencies of single-layer, dual-layer and multi-layer clouds from the GFS model for the 2 months are 68.94 % (67.11 %), 27.12 % (28.40 %), and 3.94 % (4.49 %), respectively. Overall, the GFS model produced sound frequencies of single-layer and multi-layer clouds. The

MODIS-CL results are less than those in January and July of 2001 obtained earlier by Chang and Li (2005b) for which the frequencies of cirrus overlapping lower clouds over ocean and land is 25 % (23 %) and 32 % (23 %) in January (July), respectively (Chang and Li 2005b). The differences in the frequencies of occurrence of dual-layer clouds from C–C satellites and the MODIS-CL are attributed chiefly to the retrieval of the topmost cloud layer. Cirrus clouds with CODs greater than 4.0 are classified as a single-layer cloud in the C–L algorithm. This explains why the occurrence frequencies of single-layer clouds from the MODIS-CL are greater than those from C–C satellites. The GFS model results are comparable with C–C satellites results as far as the identification of multi-layer cloud scenes is concerned.

**Table 1** Comparison of cloud layer statistics from GLAS (Wylie et al. 2007) and MODIS-CL (Chang and Li 2005b)

	From GLAS (%)	From MODIS (%)
Global cloud cover	70	71
Single layer cloud	43	44
Multiple layer cloud	27	27

**Table 2** Global occurrence frequencies of single-layer clouds, dual-layer clouds, and clouds with 3 or more layers from C–C satellites, the MODIS-CL retrievals, and GFS model results in January and July 2007

Number of layers	January			July		
	C–C (%)	C–L (%)	GFS (%)	C–C (%)	C–L (%)	GFS (%)
Single layer	67.50	84.41	68.94	67.89	82.86	67.11
Dual layers	26.58	15.59	27.12	25.98	17.14	28.40
Three or more layers	5.92	–	3.94	6.13	–	4.49

**Fig. 2** Latitudinal variations of the frequencies of cloud occurrence from C–C satellites and the GFS model for single and dual-layer clouds in January (left plot) and July (right plot) of 2007. The blue solid (light blue dashed) lines and red solid (orange dashed) lines represent single-layer and dual-layer clouds from C–C satellites (the GFS), respectively

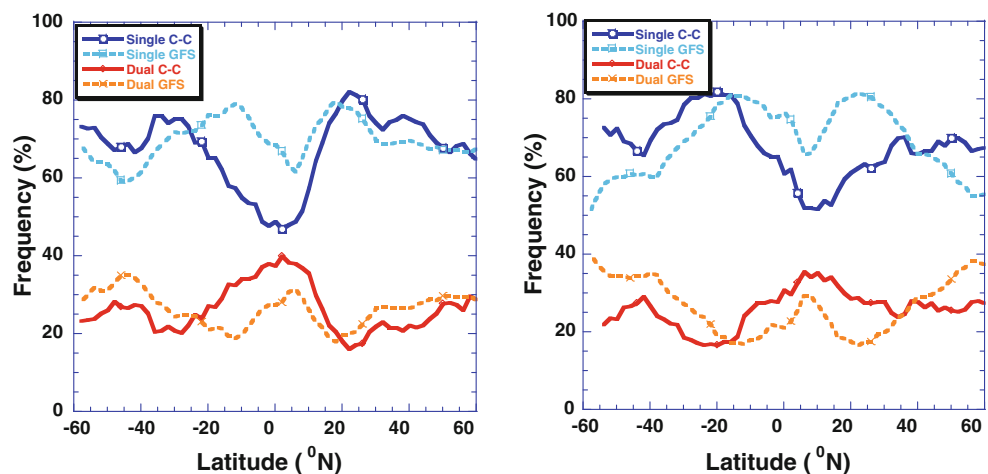


Figure 2 shows the latitudinal variations of the occurrence frequencies of zonal-mean single-layer and dual-layer cloud configurations obtained from C–C satellites and GFS model output. The patterns for single-layer cloud from observation and modeling are similar except for slight differences in their magnitudes. The C–C satellites show that dual-layer clouds occur most frequently over the inter-tropical convergence zone (ITCZ) and relatively less frequently at middle or high latitudes, relative to the GFS model results. Overall, from January (left plot in Fig. 2) to July (right plot in Fig. 2), the patterns shift with the movement of the Sun. The frequencies of occurrence of multi-layer clouds from C–C satellites in January have an oscillation that peaks around  $0^{\circ} \sim 10^{\circ}\text{N}$  with a value near 40 % and reaches a minimum of 15 % at around  $20^{\circ}\text{N}$ . The GFS model results show a maximum value of 35 % at around  $45^{\circ}\text{S}$  and a minimum value of 20 % at about  $10^{\circ}\text{S}$  and  $20^{\circ}\text{N}$ .

Figure 3 presents the latitudinal variations of the occurrence frequency of cloud layer thickness from C–C satellites and the GFS model. Both exhibit maxima in cloud layer thickness associated with deep convective clouds in the Tropics and mid-latitude continental clouds. The GFS model generally overestimates cloud layer thickness, particularly for deep convective clouds in the tropical regions and mid-latitude storm track regions. The GFS model also tends to miss very thin clouds (cloud layer thicknesses less than 2 km) that are captured in C–C satellites. Some possible causes for the different distributions of cloud layers may be either systematic biases in the prognostic cloud scheme used in the GFS model or incorrect input variables. Another possible cause of these discrepancies could be uncertainties in cloud overlapping. Depending on which cloud overlapping schemes are used in cloud fraction, results could be substantially different. Investigation of potential model errors is a subject of a companion paper.

### 3.3 Cloud fraction

Several typical cloud types are present in the lowest part of the atmosphere, such as stratus, shallow cumulus, and stratocumulus (Kuettner 1971; Agee 1984). At high levels, clouds are more associated with synoptic weather systems, like mid-latitude fronts, cyclones, tropical storms, and anvils (Starr and Cox 1985; Sheu et al. 1997). In the middle of the atmosphere ( $\sim 500\text{--}600$  mb), minimal cloud amounts were found in the tropical region from the TOGA COARE (Zuidema 1998) and from the global satellite remote sensing product of Chang and Li (2005b), as well as from the analysis of ground-based measurements (Xi et al. 2010).

Figures 4, 5 show the distributions of high, middle, and low-level marine clouds fractions from C-C satellites, MODIS-CL, and the GFS model in January and July 2007.

In general, the GFS model generates more clouds at all levels than does the C-L algorithm during the 2 months, except for low-level marine clouds (see Table 3). Middle-level cloud fractions from the GFS model are most comparable with the two satellite retrievals, as shown in Figs. 4 and 5, but large discrepancies exist in low-level clouds. In particular, more boundary layer clouds are generated by the GFS model over the interior continents at high latitudes whereas satellite retrievals show more marine stratus clouds over oceans. GFS model simulations also miss low-level shallow stratus clouds along the west coast of North America, South America, and southwestern Africa and overestimate thick, large-scale clouds associated with storm track regions. This finding is also found in a previous study that such shallow convective clouds simulated by the GFS model are entirely missed in the lower troposphere (Yang et al. 2006).

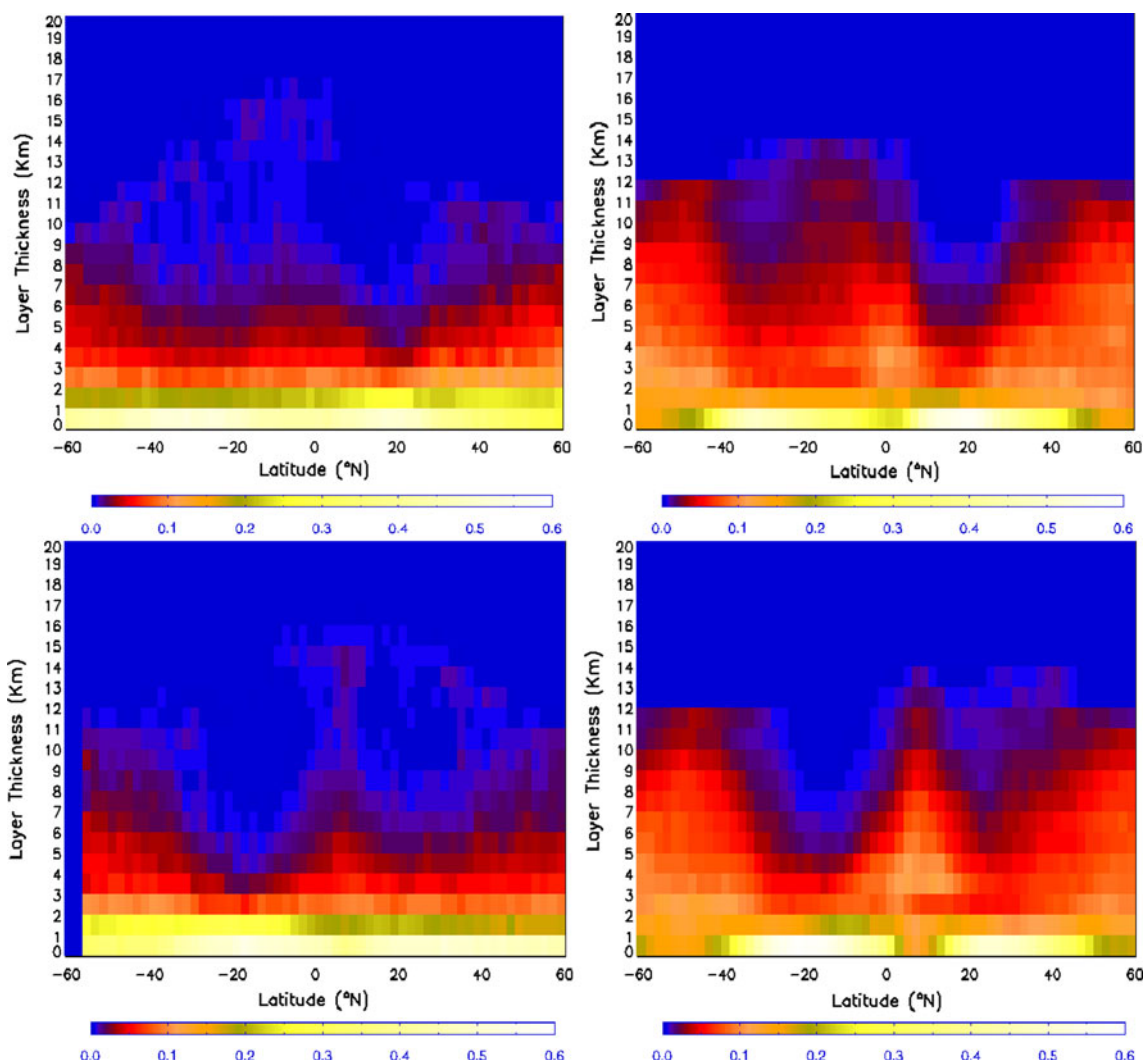


**Fig. 3** The latitudinal and vertical distributions of the frequency of occurrence (denoted by the different colors) of cloud layer thickness from C-C satellites (left plots) and the GFS model (right plots),

averaged over  $2^\circ$  latitudinal bands for January (top panels), and July (bottom panels) 2007

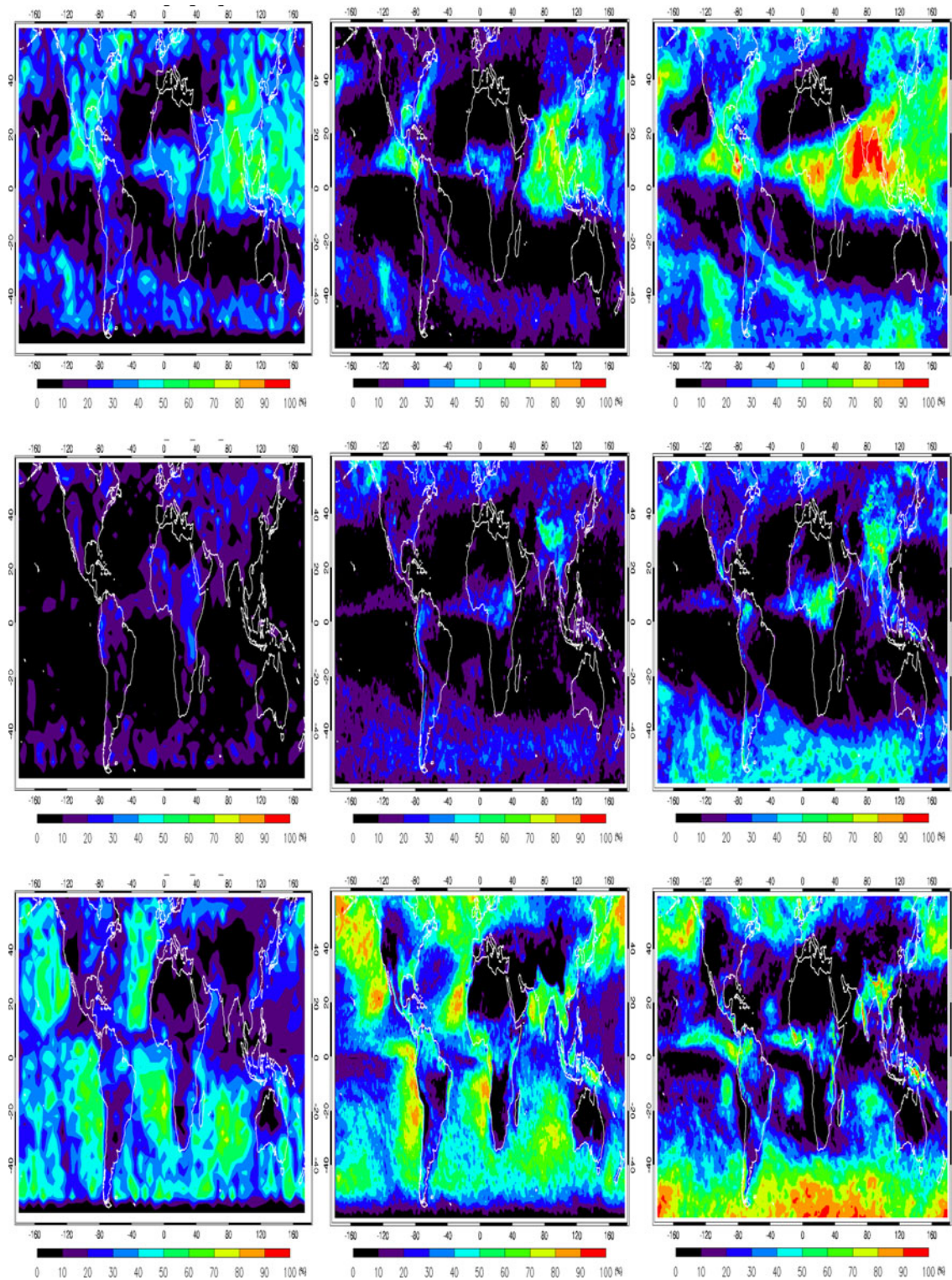


**Fig. 4** Geographic distributions of monthly mean cloud fractions from C–C satellites (*left panels*), the MODIS-CL (*middle panels*), and the GFS model (*right panels*) in July 2007. *Top, middle, and bottom plots* denote high, middle, and low clouds, respectively

The global mean mid-level cloud fraction simulated by the GFS model in January was 22.79 %, which is 6 % more than the magnitude of that retrieved by the C–L algorithm

(17.05 %). In comparison, the global mean value of mid-level cloud fraction from ISCCP is 18.0 % (Jin et al. 1996), which includes the inevitable misclassification of

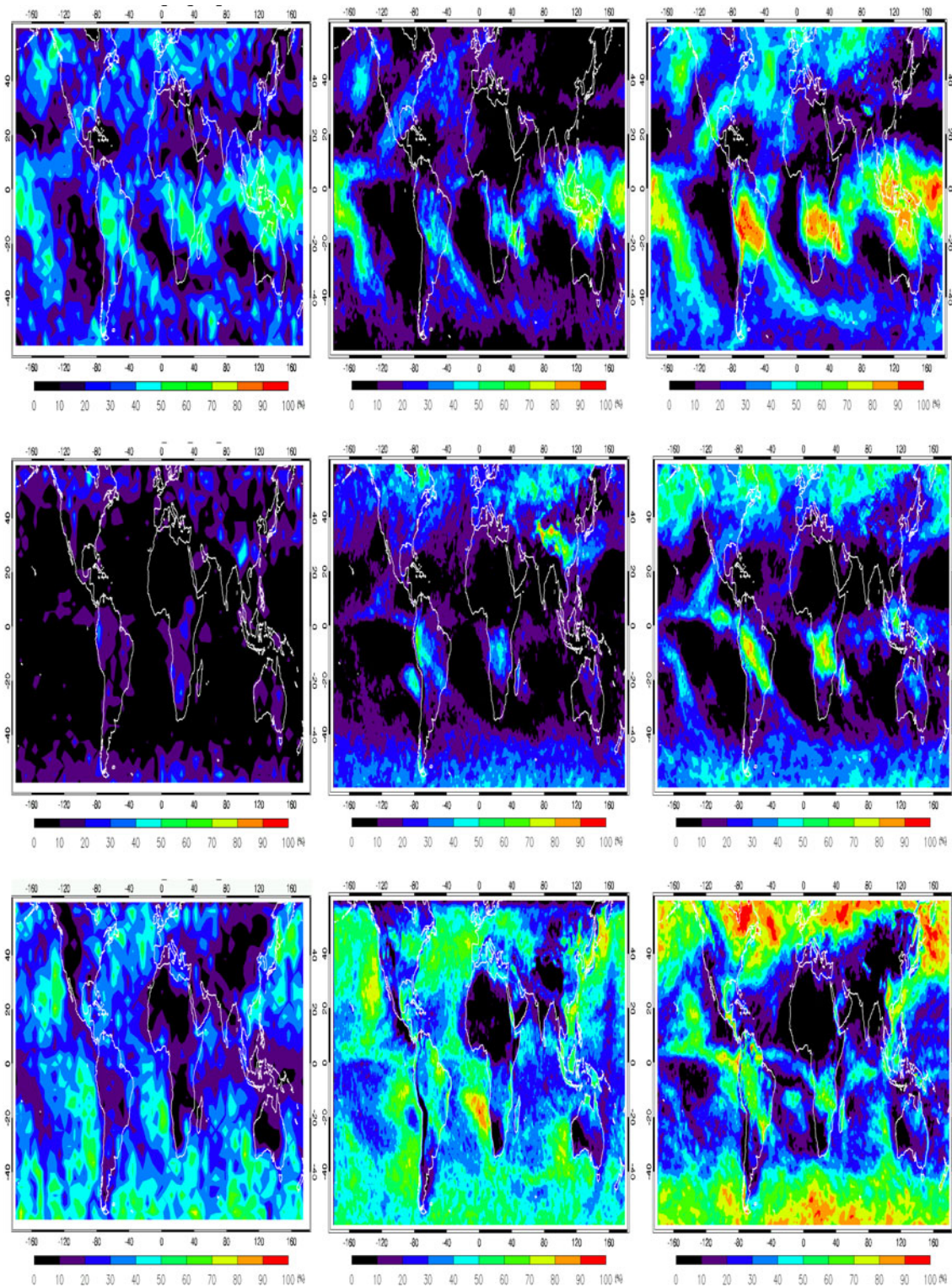


**Fig. 5** Same as Fig. 4 except for January 2007

overlapped cirrus over low water clouds as single-layer mid-level clouds. It should be emphasized that mid-level clouds in the ISCCP are defined between 440 and 680 mb while those in the GFS model are between 350 and 642 mb. The

mid-level cloud fraction retrieved from the C-L algorithm using the ISCCP criterion is about 9–10 % (not shown). We can thus affirm that the GFS model overestimates mid-level clouds. The global mean cloud fraction of low-level clouds

from the GFS model was 39.24 %, which is similar to that from the C–L algorithm in January (38.98 %) although the spatial patterns differ (see Figs. 4, 5).

To examine the global distribution patterns of clouds, three separate geographical regions are defined in order to identify areas of the largest differences in cloud fraction: tropical (20°S–20°N), mid-latitude (20°N–40°N, 20°S–40°S), and high latitude (40°N–60°N, 40°S–60°S). Differences were calculated by subtracting GFS results from the C–L algorithm retrievals; the numbers in Table 4 are zonally-averaged cloud fractions over 2° latitudinal bins. The GFS model cloud fractions at high latitudes for all levels are greater than those from satellite retrievals. In particular, the GFS model simulates too much boundary layer clouds at high latitudes. At mid-latitudes (the Tropics), the GFS-forecasted high cloud fractions in January are greater than those retrieved from satellite by 10.87 % (14.10 %) and 2.01 % (7.25 %) for mid-level clouds, but low cloud fractions are less by 9.40 % (7.91 %).

Figure 6 illustrates the latitudinal variations of zonal-mean cloud fractions corresponding to the three cloud vertical categories (i.e., high, middle, and low). Two features stand out. First, GFS model results vary in the same manner as satellite retrievals in terms of spatial features and locations except for low-level clouds. Second, modeled zonally-averaged high and mid-level cloud amounts are generally overestimated over nearly all latitudinal bands. Variations of high-level clouds from both the C–L

algorithm and the GFS model show the jump in cloud amount in the Tropics of the Northern Hemisphere from January to July due to deep convective clouds and the decrease in high-level cloud amount in subtropical regions in the Southern Hemisphere. For mid-level clouds, the GFS model captures the July reduction in cloud amount between 20 and 5°S but overestimates cloud amounts in the Northern Hemisphere. Low cloud fractions generated by the GFS model diverge remarkably from satellite retrievals. Note that the C–L algorithm results in July show a sharp decrease in cloud fractions at around 55°S. This is because the C–L algorithm uses solar zenith angle (SZA) information for detecting clouds. When the SZA is larger than a specific threshold value (e.g., 80°), no retrievals are made. Simulations of cloud from the GFS model do not explicitly involve sunlight information, so clouds can be seen over those particular regions.

### 3.4 Liquid water path (LWP) and ice water path (IWP)

Cloud LWP/IWPs are estimated from both MODIS-CL and the GFS model during the daytime. The modeled LWP is based on the cloud water mixing ratio at each level and the observed LWP is retrieved from the C–L algorithm using the MODIS data. The MODIS-CL LWP/IWPs are calculated using cloud optical depth and a fixed effective radius of 10 μm (30 μm) for water (ice) clouds and they are more reliable than those from the MODIS-EOS products because the C–L algorithm retrievals include overlapped low clouds beneath high clouds.

The spatial distributions of modeled and satellite-retrieved LWPs for January and July 2007 are shown in Figs. 7 and 8. The LWP of high-level clouds simulated from the GFS model is substantially smaller than that retrieved from satellite measurements in both January and July. For mid-level, GFS and MODIS-CL LWPs in January showed quite different distribution patterns. The GFS-modeled LWP was more over South America, the southern parts of Africa, and in some parts of South Asia, but it was

**Table 3** Global monthly mean high-, mid-, and low-level cloud fractions obtained from the C–L algorithm and the GFS model during January and July 2007

	C–L algorithm		GFS	
	January (%)	July (%)	January (%)	July (%)
High	16.45	16.36	30.61	32.90
Mid	17.05	13.61	22.79	19.46
Low	38.98	37.11	39.24	31.15

**Table 4** Zonally-averaged cloud fraction (and differences) from the MODIS-CL and the GFS model in January and July 2007

	January			July		
	40°–60° –40° to –60°	20°–40° –20° to –40°	–20°–20°	40°–60° –40° to –60°	20°–40° –20° to –40°	–20°–20°
High	12.52/30.36	13.96/24.83	23.84/37.95	13.82/34.30	14.16/24.58	21.46/40.60
Diff	–17.83	–10.87	–14.10	–20.48	–10.42	–19.14
Mid	27.37/35.84	13.28/15.30	10.20/17.45	20.82/32.49	11.17/14.78	8.72/10.92
Diff	–8.47	–2.01	–7.25	–11.67	–3.62	–2.20
Low	43.31/61.52	38.12/28.72	35.24/27.33	39.94/51.23	37.19/21.99	34.04/20.14
Diff	–18.21	9.40	7.91	–11.28	15.20	13.90

Differences are calculated as the C–L algorithm results minus GFS model results

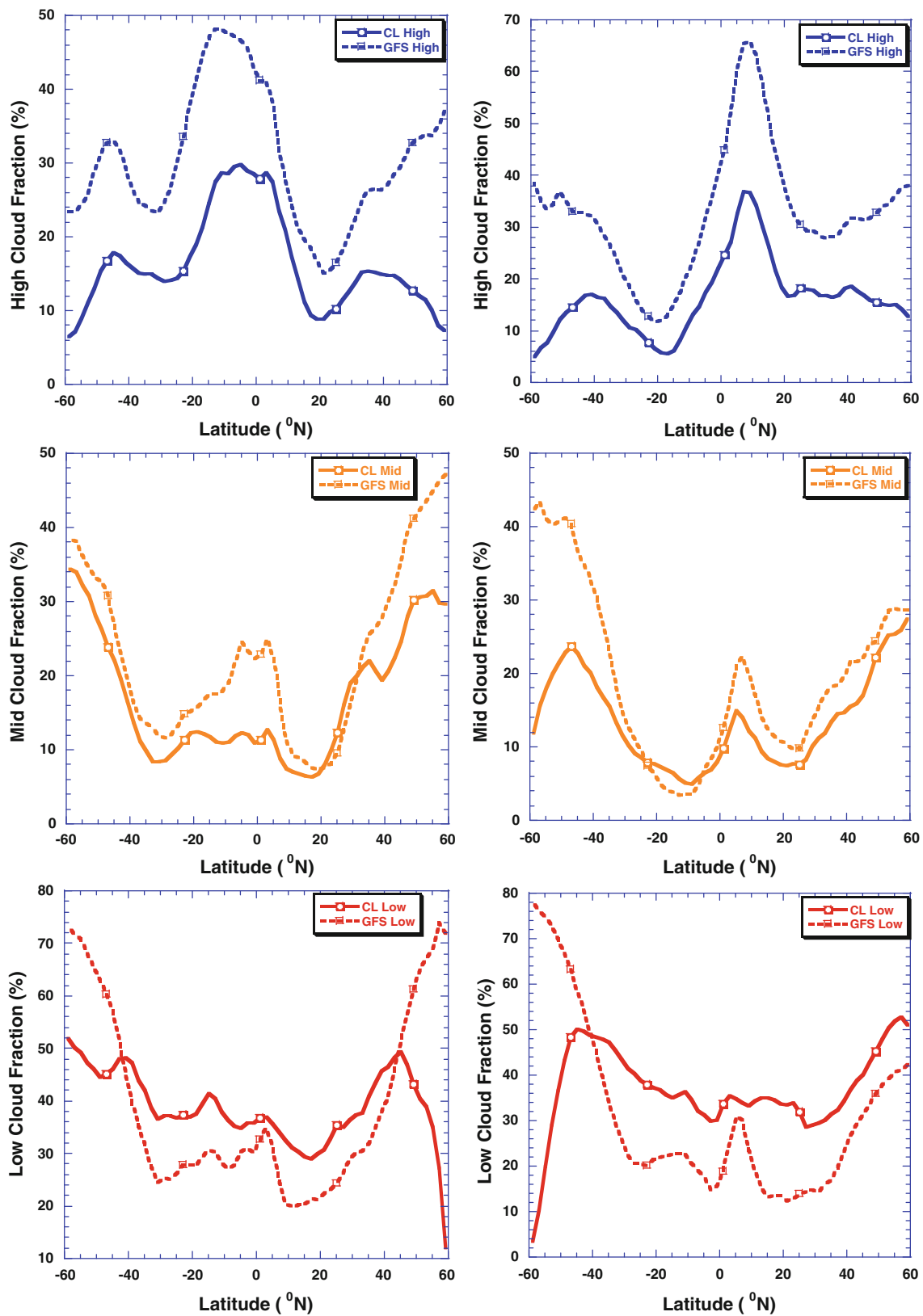


**Fig. 6** Latitudinal variations of cloud fraction for high clouds (*top plots*), middle clouds (*middle plots*), and low clouds (*bottom plots*) in January (*left*) and July (*right*) 2007. *Solid lines* and *dashed lines* represent results from the C-L algorithm and the GFS model, respectively

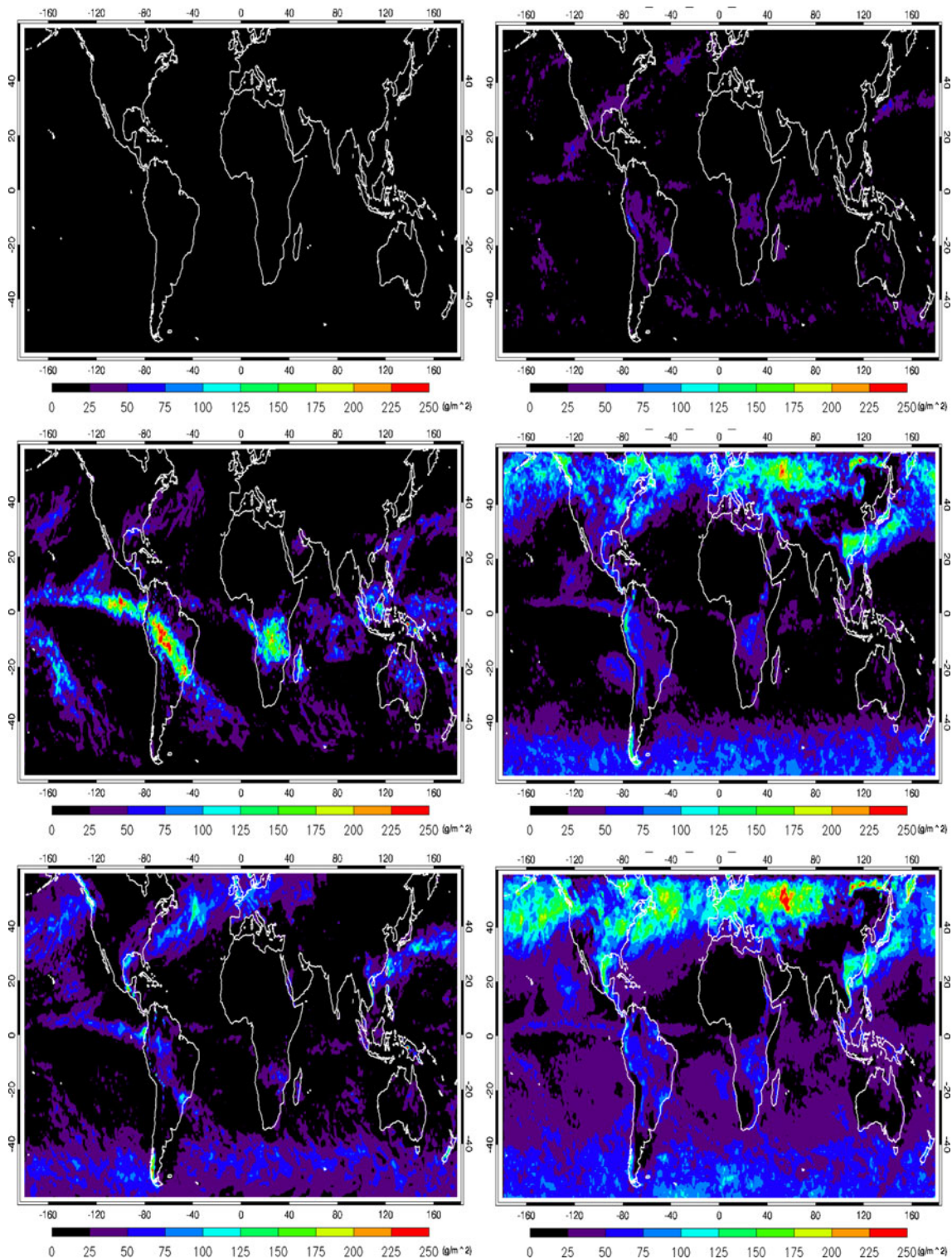


**Fig. 7** LWP from the GFS model (*left plots*) and MODIS-CL (*right plots*) in January 2007. *Upper, middle, and bottom sets* of figures represent high, mid, and low-level LWPs, respectively. Units are in  $\text{g/m}^2$

mostly missed over North America, Europe, and the East Asia region relative to the satellite retrievals. The low-level LWP from the MODIS-CL retrievals was significantly greater than that simulated by the GFS model, particularly

over oceans and at high latitudes in both hemispheres. These features are also evident in July.

Figures 9 and 10 show near-global distributions of monthly mean IWPs obtained from both the MODIS-CL

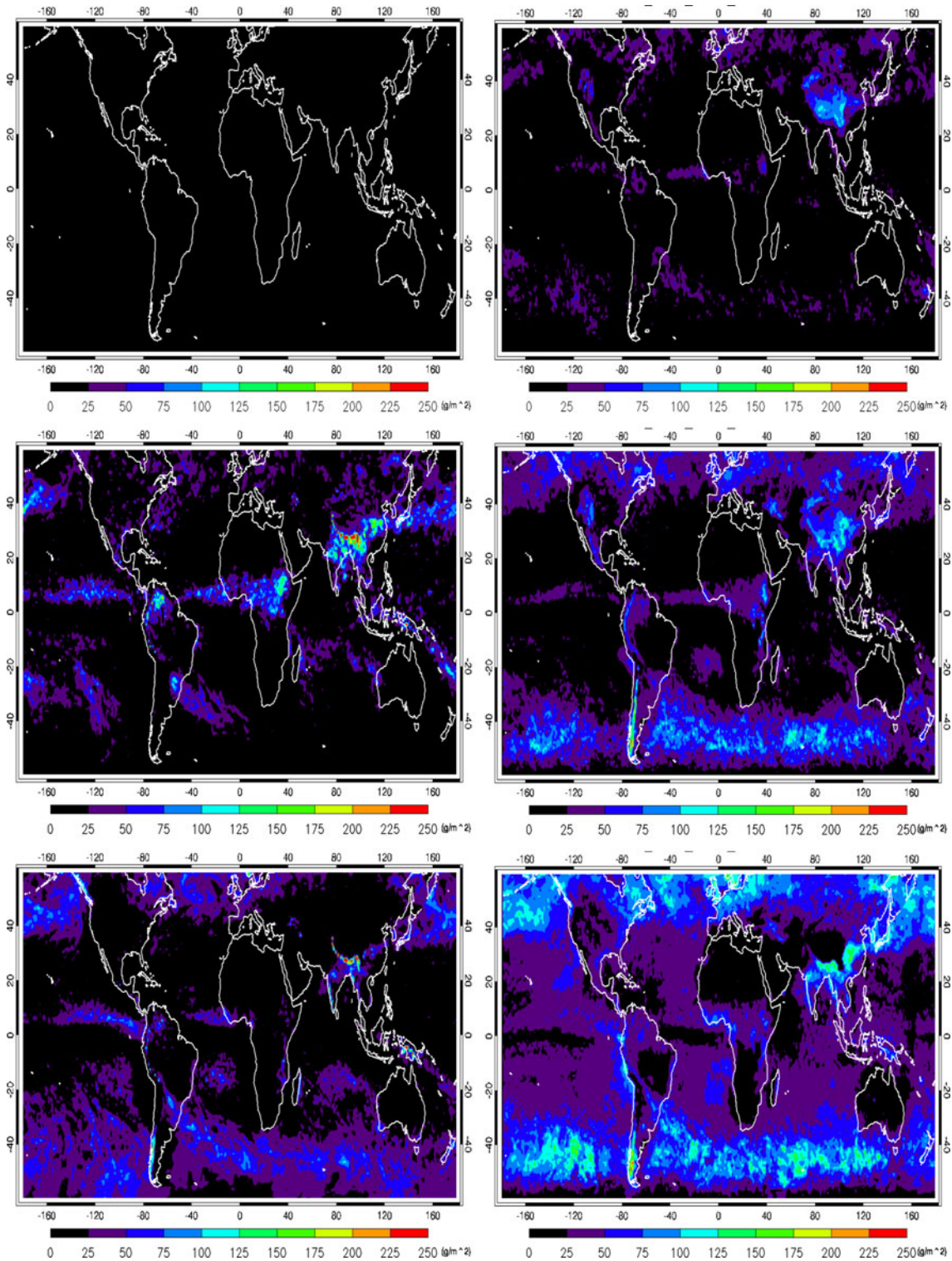


**Fig. 8** Same as Fig. 7 except for July 2007

retrievals and the GFS model in January and July 2007. In general, the GFS model produces more IWP in the Tropics but agrees in spatial distribution with the satellite retrievals. GFS simulations of high-level IWP are smaller than

the MODIS-CL IWP retrievals over the North Atlantic Ocean, the northeastern Pacific Ocean, and the East Asia region during January and over the Southern Ocean during July. The spatial distributions of mid- and low-level IWP

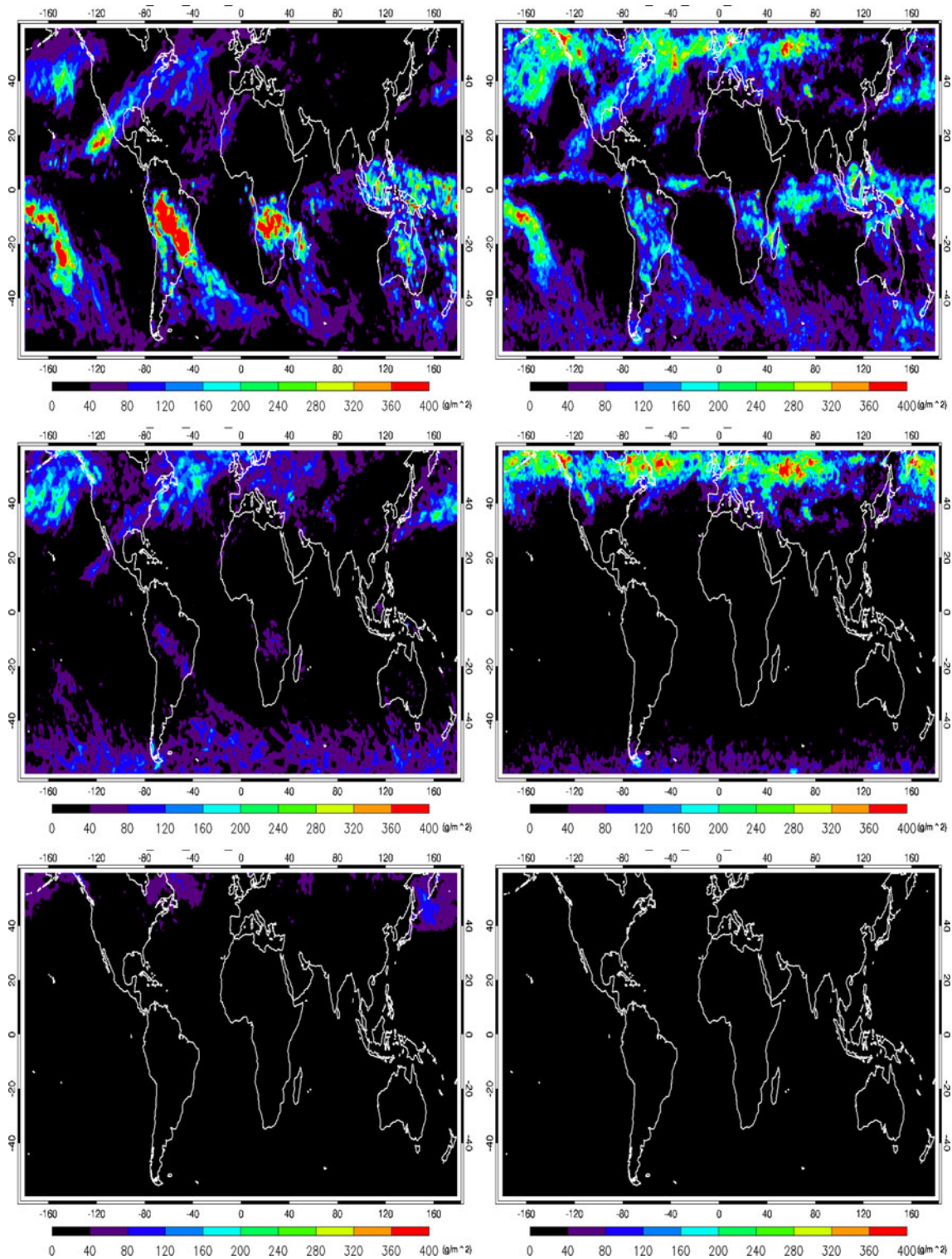


**Fig. 9** IWP from the GFS model (*left plots*) and MODIS-CL (*right plots*) in January 2007. *Upper, middle, and bottom sets* of figures represent high, mid, and low-level IWPs, respectively. Units are in  $\text{g/m}^2$

from both model and satellite are generally comparable, although the mid-level IWP generated by the GFS model is somewhat underestimated beyond  $40^\circ\text{N}$  toward polar

region during January. Except in high latitude regions, very little low-level IWP is seen from both model and observation.

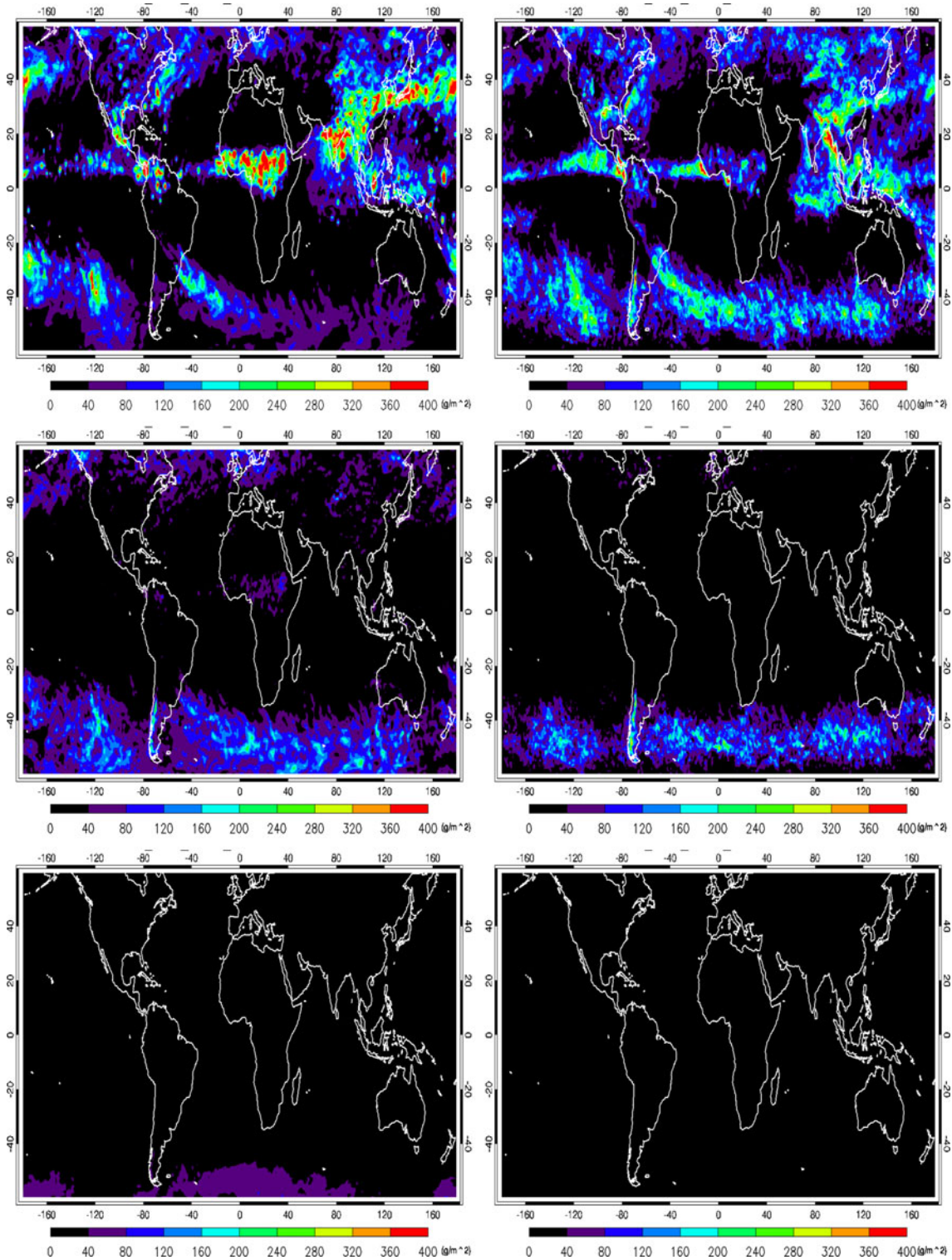


**Fig. 10** Same as Fig. 9 except for July 2007

Cloud fraction and LWP/IWPs generated by the GFS model strongly depend on the cloud water mixing ratio variable. In the current GFS model, cloud water mixing ratio is the sole predictor of LWP/IWPs and the primary

predictor of cloud fraction. We can conjecture the causes for the systematic model errors, without dealing with many complex issues related to cloud modeling. The findings suggest that the cloud water mixing ratio cannot represent

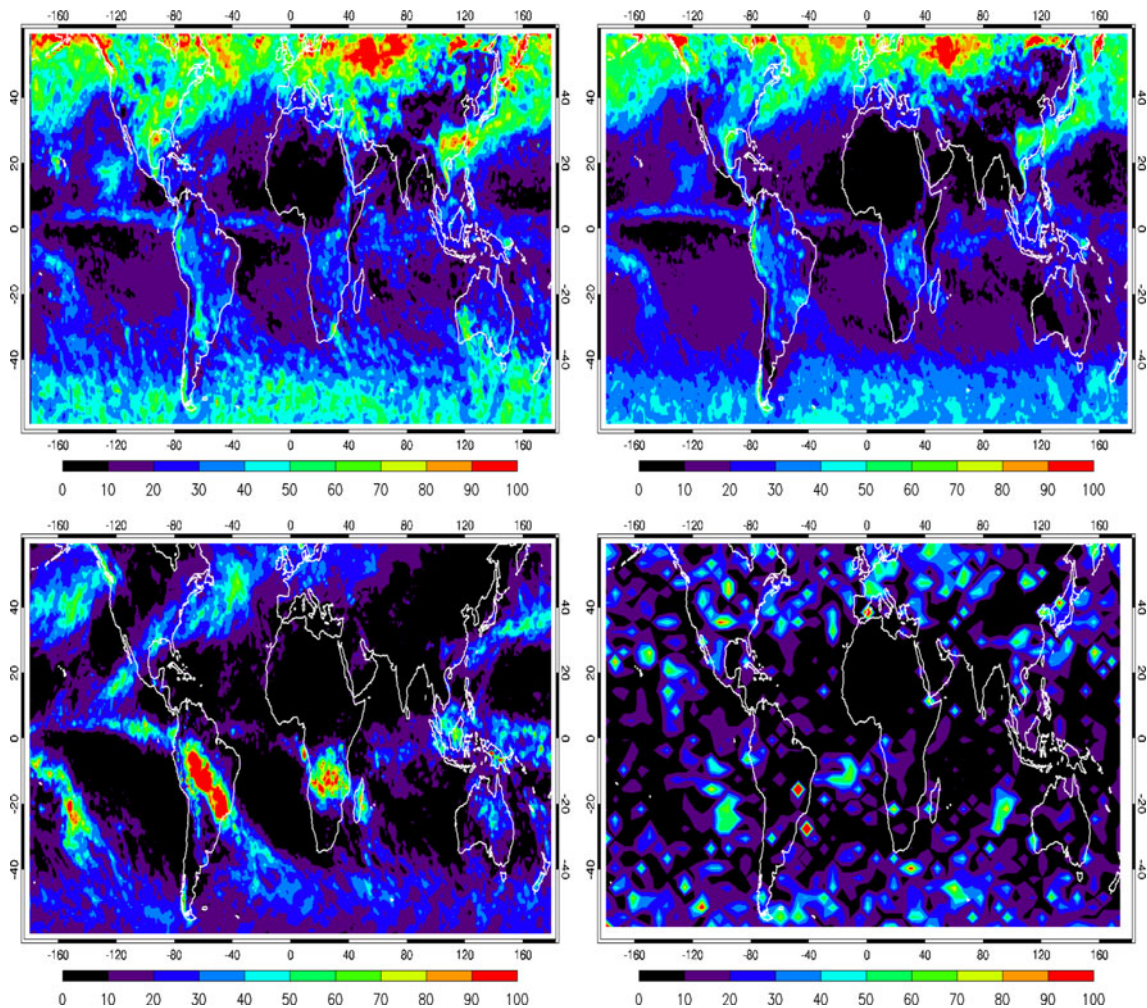


**Fig. 11** Total COD from (clockwise, starting from the *upper left plot*) the MODIS-CL, MODIS-EOS, CloudSat, and the GFS model during January 2007

cloud formation well in the lower troposphere. As noted in other studies (Sun et al. 2010; Han and Pan 2011), the GFS model has a systematic error in shallow convective scheme. A strong turbulent diffusion removes condensed water in the lower troposphere, which leads to an underestimation of low clouds and low-level LWP. Furthermore, it potentially allows for excessive downward shortwave fluxes and less longwave fluxes at the surface.

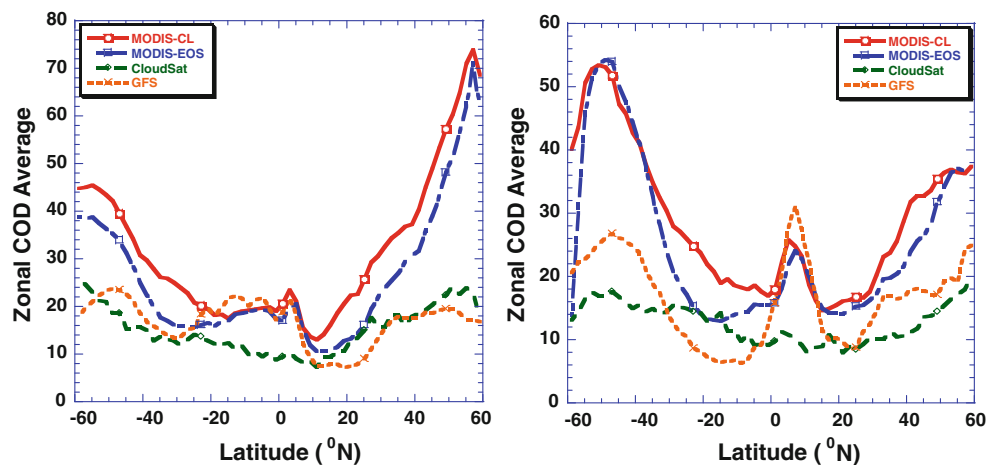
### 3.5 Cloud optical depth (COD)

The properties of clouds as well as the presence of clouds need to be considered in evaluating clouds simulated by models (Klein and Jakob 1999). Global distributions of COD obtained from different sources are shown in Figs. 11 and 12. The upper plots in Fig. 11 represent retrievals from the same data but using different algorithms (the C-L algorithm on the left and the MODIS-EOS algorithm on the right); patterns are similar between the two retrievals but

magnitude of COD from the MODIS-CL retrievals is larger than that from the MODIS-EOS retrievals on a global scale. This is a result of the recovery of low clouds overlapped with high clouds. The two MODIS-based CODs are generally prevalent in mid-latitude storm track regions during January. The GFS model can simulate the general pattern of observed CODs but the magnitudes are too small over those regions. Overestimation of COD is seen over South America and the southern portion of Africa; the modeled-COD is underestimated over the Southern Ocean.

Regarding CloudSat results, Kahn et al. (2007) reported that thin cirrus cloud retrievals from the radar-only scheme had some differences with retrievals from the combined radar-lidar scheme. Optically thin clouds are undetected when using the radar-only cloud scheme because of the existence of small ice particles. Also, low clouds below 1 km are difficult to be detected with the radar-only scheme due to ground clutter issues. This shows that CloudSat is not as sensitive to thin cirrus and boundary

**Fig. 12** Latitudinal variations of COD in January (*left plot*) and July (*right plot*) 2007. The *solid red lines*, *dash-dotted blue lines*, *dashed green lines*, and *dotted orange lines* represent results from the MODIS-CL, MODIS-EOS, CloudSat, and the GFS model, respectively



layer clouds. So CloudSat retrievals of COD are underestimated over most areas of the globe. The lidar is more sensitive than the radar to small hydrometeors, such as small ice crystals and water droplets, but is not capable of detecting clouds at lower levels of the atmosphere because it cannot penetrate through clouds all the way to the surface. Lidar COD retrievals range from 0 to 5 only and C–C satellites do not provide COD retrievals. Therefore, more reliable active sensor datasets such as C–C satellites retrievals are required in the future so that more accurate verification of COD retrievals can be performed.

Figure 12 shows the latitudinal variations of monthly mean COD distributions from MODIS-EOS, MODIS-CL, CloudSat, and the GFS model during January (left plot) and July (right plot). Averages were taken over  $2^\circ$  latitudinal bins. The C–L algorithm results are more than results from the MODIS-EOS algorithm in most areas for the 2 months. The GFS model significantly underestimates COD except in the Tropics in January. Within these regions, COD retrievals from the GFS model are around 2–3 times less than the MODIS-based retrievals. Two peaks in both of the MODIS products are seen near  $50^\circ\text{S}$  and  $5^\circ\text{N}$  in July, corresponding to clouds from storm tracks in the Southern Hemisphere and convective clouds in the ITCZ. Zonally-averaged CODs generated by the GFS model in July are less than satellite retrievals of COD in the entire Southern Hemisphere. Zonally-averaged CODs from CloudSat retrievals are generally much smaller than the other satellite-based retrievals/model results during January and July. In brief, the GFS model somewhat overestimated COD in the Tropics where deep convective clouds are dominant and substantially underestimated COD over storm track regions and subtropical regions of the world.

Systematic forecast errors can exist in radiation fields due to errors in the simulations of cloud properties in the boundary layer. In a previous study with a single column model including the GFS physical processes, it was found

that modeled downward shortwave fluxes were significantly overestimated while sensible heat fluxes were underestimated at the surface (Yang et al. 2006). To understand the causes for the discrepancies in radiative fluxes, cloud parameters such as effective droplet radius and cloud optical depth need to be evaluated.

#### 4 Summary and discussion

Clouds and their interactions with large-scale atmospheric circulation are crucial parts of weather and climate systems. So far, we have a poor understanding of how well clouds are simulated by weather forecast and climate models due to limited reliable observations, especially concerning the vertical distribution of clouds. However, the advent of advanced remote sensing technique in the recent decade allows us to assess and improve cloud fields in terms of both horizontal and vertical variations.

In this study, we employed multiple global satellite products from the A-Train constellation to evaluate clouds generated by the NCEP GFS model. Cloud properties simulated by the GFS model are compared with satellite retrievals from CloudSat, CloudSat-CALIPSO merged data, MODIS-EOS, and a new MODIS-based research product developed by Chang and Li (2005a, b). Extensive cloud variables are assessed including the frequencies of cloud layers occurrence, cloud fraction and thickness, cloud optical depth, liquid water path, and ice water path. In particular, an evaluation of the GFS cloud vertical structure on a global scale is the main focus of this study.

The GFS model captures well the spatial distributions of hydrometeors, which bear a reasonable resemblance to those seen from satellite retrievals, although large differences exist in magnitude. The GFS model generates more high-level and mid-level clouds, but less low-level clouds than do satellite retrievals. More boundary layer clouds

over the interior of continents at high latitudes were generated by the GFS model whereas satellite retrievals showed more low clouds over oceans. In other words, the GFS model tends to miss low-level marine stratocumulus clouds and overestimate interior continental low-level clouds. GFS-modeled CODs are less than those from MODIS retrievals in high latitude regions of both hemispheres and are overestimated over South America and the southern African region during January 2007. The GFS model overproduces COD values in deep convective cloud regimes and simulates much less COD values in subtropical regions. GFS-modeled IWP distributions agree better with satellite retrievals than do LWP distributions.

These comparisons provide useful guidance toward diagnosing the source of possible errors, especially with regard to systematic biases that help identify major flaws in either cloud parameterization schemes or input variables, or both. More thorough and rigorous investigations into causes of the discrepancies are addressed in a separated paper by means of model sensitivity tests, analysis of various input variables used in the GFS cloud parameterization schemes, and further validation of these variables. More independent satellite products such as atmospheric profiles of temperature and moisture from microwave radiometers will also be employed to help understand the discrepancies.

**Acknowledgments** This study is supported by NOAA through CICS, MOST (2013CB955804), NASA (NNX08AH71G) and DOE (DESC0007171), and with helps from Drs. Yu-Tai Hou, Brad Ferrier, Shrinivas Moorthi, and Steve Lord from the NOAA/National Center for Environmental Prediction (NCEP).

## References

- Agee EM (1984) Observations from space and thermal convection: a historical perspective. *Bull Am Meteor Soc* 65:938–949
- Barnes WL, Pagano TS, Salomonson VV (1998) Prelaunch characteristics of the moderate resolution imaging spectroradiometer (MODIS) on EOS-AM1. *IEEE Trans Geosci Remote Sens* 36:1088–1100
- Baum BA, Spinhirne JD (2000) Remote sensing of cloud properties using MODIS airborne simulator imagery during SUCCESS. 3. Cloud overlap. *J Geophys Res* 105:11793–11804
- Baum BA, Uttal T, Poellot M, Ackerman TP, Alvarez JM, Intrieri J, Starr DO'C, Titlow J, Tovinkere V, Clothiaux E (1995) Satellite remote sensing of multiple cloud layers. *J Atmos Sci* 52:4210–4230
- Bodas-Salcedo A, Webb MJ, Brooks ME, Ringer MA, William KD, Milton SF, Wilson DR (2008) Evaluating cloud systems in the Met Office global forecast model using simulated CloudSat radar reflectivities. *J Geophys Res* 113:D00A13. doi:10.1029/2007JD009620
- Chang FL, Li Z (2005a) A new method for detection of cirrus-overlapping-low clouds and determination of their optical properties. *J Atmos Sci* 62:3993–4009
- Chang FL, Li Z (2005b) A near global climatology of single-layer and overlapped clouds and their optical properties retrieved from TERRA/MODIS data using a new algorithm. *J Clim* 18:4752–4771
- Chou MD, Suarez MJ, Ho CH, Yan HMM, Lee KT (1998) Parameterizations for cloud overlapping and shortwave single scattering properties for use in general circulation and cloud ensemble models. *J Clim* 11:202–214
- Han J, Pan HL (2011) Revision of convection and vertical diffusion schemes in the NCEP global forecast system. *Wea Forecast* 26:520–533
- Harshvardhan RD, Randall DA, Corsetti TG, Dazlich DA (1989) Earth radiation budget and cloudiness simulations with a general circulation model. *J Atmos Sci* 46:1922–1942
- Heymsfield AJ, McFarquhar GM (1996) High albedos of cirrus in the tropical pacific warm pool: microphysical interpretations from CEPEX and from Kwajalein, Marshall Islands. *J Atmos Sci* 53:2424–2451
- Im E, Durden SL, Wu C (2006) Cloud profiling radar for the CloudSat mission. *IEEE Aerosp Electron Syst Mag* 20:15–18
- Jin Y, Rossow WB, Wylie DP (1996) Comparison of the climatologies of high-level clouds from HIRS and ISCCP. *J Clim* 9:2850–2879
- Kahn BH, Chahine MT, Stephens GL, Mace GG, Marchand RT, Wang Z, Barnet CD, Eldering A, Holz RE, Kuehn RE, Vane DG (2007) Cloud type comparisons of AIRS, CloudSat, and CALIPSO cloud height and amount. *Atmos Chem Phys Discuss* 7:13915–13958
- Klein SA, Jakob C (1999) Validation and sensitivities of frontal clouds simulated by the ECMWF model. *Mon Wea Rev* 127:2514–2531
- Kuettner JP (1971) Cloud bands in the earth's atmosphere. *Tellus* 23:404–425
- Li Z, Leighton H (1991) Scene identification and its effect on cloud radiative forcing in the Arctic. *J Geophys Res* 96:9175–9188
- Mace GG et al (2006) Cloud radiative forcing at the atmospheric radiation measurement program climate research facility: 1. Technique, validation, and comparison to satellite derived diagnostic quantities. *J Geophys Res* 111:D11S90. doi:10.1029/2005JD005921
- Mace GG, Zhang Q, Vaughn M, Marchand R, Stephens G, Trepte C, Winker D (2009) A description of hydrometeor layer occurrence statistics derived from the first year of merged Cloudsat and CALIPSO data. *J Geophys Res* 114:D00A26. doi:10.1029/2007JD009755
- Ou SC, Liou KN, Baum BA (1996) Detection of multilayer cirrus cloud systems using AVHRR data: verification based on FIRE-II IFO composite measurements. *J Appl Meteorol* 35:178–191
- Pincus R, Platnick S, Ackerman S, Hemler R, Hofmann R (2012) Reconciling simulated and observed views of clouds: MODIS, ISCCP, and the limits of instrument simulators. *J Clim*. doi:10.1175/JCLI-D-11-00267.1
- Platnick S, King MD, Ackerman SA, Menzel WP, Baum BA, Riedi JC, Frey RA (2003) The MODIS cloud products: algorithms and examples from Terra. *IEEE Trans Geosci Remote Sens* 41:459–473
- Sassen K, Wang Z (2008) Classifying clouds around the globe with the CloudSat radar: 1-year of results. *Geophys Res Lett* 35:L04805. doi:10.1029/2007GL032591
- Sheu RS, Curry JA, Liu G (1997) Vertical stratification of tropical cloud properties as determined from satellite. *J Geophys Res* 102:4231–4245
- Starr DO'C, Cox SK (1985) Cirrus clouds. Part II: numerical experiments on the formation and maintenance of cirrus. *J Atmos Sci* 42:2682–2694
- Stephens GL (2005) Cloud feedbacks in the climate system: a critical review. *J Clim* 18:237–273

- Stephens GL, Vane DG, Boain RJ, Mace GG, Sassen K, Wang Z, Illingworth AJ, O'Connor EJ, Rossow WB, Durden SL, Miller SD, Austin RT, Benedetti A, Mitrescu C (2002) The cloudsat mission and the A-train. *Bull Am Meteorol Soc* 83:1771–1790
- Sun R, Moorthi S, Xiao H, Mechoso CR (2010) Simulation of low clouds in the Southeast Pacific by the NCEP GFS: sensitivity to vertical mixing. *Atmos Chem Phys* 10:12261–12272. doi: [10.5194/acp-10-12261-2010](https://doi.org/10.5194/acp-10-12261-2010)
- Weare BC, AMIP Modeling Groups (1996) Evaluation of the vertical structure of zonally averaged cloudiness and its variability in the atmospheric model intercomparison project. *J Clim* 9:3419–3431
- Winker DM, Hunt WH, McGill MJ (2007) Initial performance assessment of CALIOP. *Geophys Res Lett* 34:L19803. doi: [10.1029/2007GL030135](https://doi.org/10.1029/2007GL030135)
- Wylie D, Eloranta E, Spinhirne JD, Palm SP (2007) A comparison of cloud cover statistics from the GLAS lidar with HIRS. *J Clim* 20:4968–4981. doi: [10.1175/JCLI4269.1](https://doi.org/10.1175/JCLI4269.1)
- Xi B, Dong X, Minnis P, Khaiyer MM (2010) A 10 year climatology of cloud fraction and vertical distribution derived from both surface and GOES observations over the DOE ARM SGP site. *J Geophys Res* 115:D12124. doi: [10.1029/2009JD012800](https://doi.org/10.1029/2009JD012800)
- Xu KM, Randall DA (1996) A semiempirical cloudiness parameterization for use in climate models. *J Atmos Sci* 53:3084–3102
- Yang F, Pan HL, Krueger SK, Moorthi S, Lord SJ (2006) Evaluation of the NCEP global forecast system at the ARM SGP site. *Mon Wea Rev* 134:3668–3690
- Zhang MH et al (2005) Comparing clouds and their seasonal variations in 10 atmospheric general circulation models with satellite measurements. *J Geophys Res* 110:D15S02. doi: [10.1029/2004JD005021](https://doi.org/10.1029/2004JD005021)
- Zuidema P (1998) The 600–800 mb minimum in tropical cloudiness observed during TOGA COARE. *J Atmos Sci* 55:2220–2228